https://doi.org/10.48047/AFJBS.6.16.2024.3574-3598

African Journal of Biological Sciences

Journal homepage: http://www.afjbs.com

Research Paper Open Access

Antibacterial and Antioxidant Properties of Iron Oxide Nanoparticles and Targeted Effects on Surface Proteins of *Staphylococcus aureus* By *In Silico* Methods

Abiyoga M[1], Saravana kumari P [1]*, Bhuvaneshwari K[2], Sreelakshmi S[2], Anjana M I[3]

[1]Department of Microbiology, RVS College of Arts and Science, Coimbatore, India. ORCiD - 0009-0008-2051-0004 abiyoga413@gmail.com
[2]Department of Microbiology, Tiruppur kumaran college for women, Tiruppur, India.bhuvaneshwarikrishnamurthy4@gmail.com
[2]Department of Microbiology, Tiruppur kumaran college for women, Tiruppur, India. sreeshyam2001@gmail.com
[3] Department of Microbiology, RVS College of Arts and Science, Coimbatore, India .anjana.m.i59@gmail.com

Corresponding author
Dr. P. Saravanakumari[1*], Department of Microbiology, RVS College of Arts and Science, Coimbatore, India. ORCiD- 0000-0002-5031-9859 researchinmicro@gmail.com Ph No-9442386269.

Volume 6, Issue 16, Dec 2024

Received: 15 Oct 2024

Accepted: 25 Nov 2024

Published: 09 Dec 2024

doi:10.48047/AFJBS.6.16.2024.3574-3598

Abstract
Wound infections are considered significant health care problems, leading to high morbidity and mortality globally. Because wound infections are becoming a threat due to the acquisition of antimicrobial resistance by liable pathogens. The current study aimed to analyze the effect of iron oxide nanoparticles (IONP) such pathogens to overcome the issue. IONP is chemically synthesized from ferric chloride and ferrous sulphate as raw materials and co-precipitated to ferrous oxide. Production of IONP confirmed by UV-VIS spectrophotometry at 370nm and stability determined by zeta potential. Obtained dark brown color, fine powder of IONP appeared as flakes like thin discs, with a size range of 20.41 - 36.86nm in diameter under FESEM analysis. Presence of strong Fe-O stretch documented by the FTIR analysis and confirmed the formation of IONP. Synthesized nanoparticles showed high antimicrobial activity against methicillin-resistant *Staphylococcus aureus.* MIC was identified as 31.25 µg/ml and MBC was determined as 62.5 µg/ml. Antioxidant activity of synthesized nanoparticles was identified by DPPH scavenging assay as 61.4 µg/ml. SWISS ADME and ADMETSAR studies revealed favorable pharmacological properties with non-toxicity, high blood-brain barrier (BBB) penetration, and easy absorption ability. Interaction of iron oxide nanoparticles against *Staphylococcus aureus* surface protein 3TIP and 3TIQ showed a high binding affinity of -3.4 kcal/mol. Thus this study revealed the drug candidacy of iron oxide nanoparticles against methicillin-resistant *Staphylococcus aureus*.

Keywords- Iron oxide nanoparticles, Co-precipitation method, Methicillin resistant *Staphylococcus aureus*, Molecular docking, Surface protein G

Graphical abstract

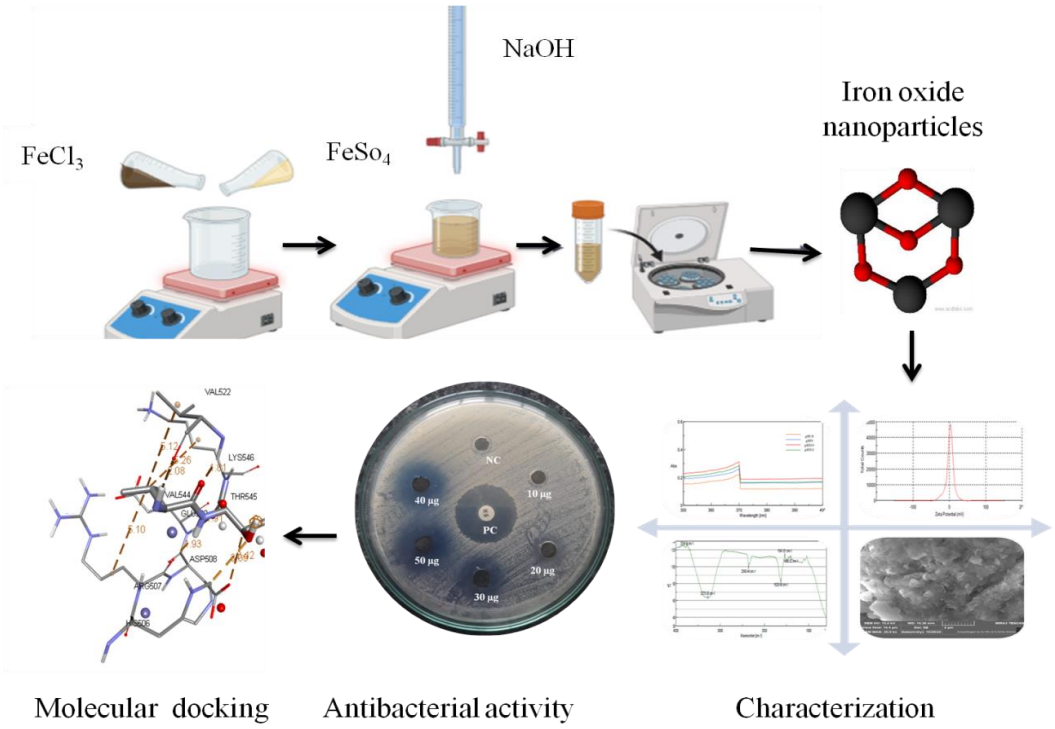

Introduction

In the clinical sector, antimicrobial resistance (AMR) is recognized as a major global threat to public health and development. Clinical data of 2021 reported that bacterial AMR was responsible for 4.71 million deaths globally, and most of the deaths connected with methicillin-resistant *Staphylococcus aureus* accounted for 1.46 million deaths in 2021. Followed by, carbapenem-resistant pathogens caused mortality of 1.3 million in 2021, and global AMR-related deaths may be expected to increase to 8.22 million in 2050 (Naghavi et al., 2024). AMR is attributed by the genetic changes in pathogens, gradually affects the genetic make-up of the organisms, and resistant genes are developed and inherited over time through inappropriate and overuse of antibiotics in humans and animals. Commonly recommended antibiotics has various side effects, including Lack of specificity, inhibition of native organisms, and reduced efficacy in patients undergoing chemotherapeutic treatments, probiotic therapies, or taking anti-diabetic medicines (Jaha et al., 2024).

Wound infections are a significant healthcare problem, leading to high morbidity and mortality worldwide. It is estimated that the prevalence of diabetic foot ulcers is 2.21 per 1000 population globally, with chronic wounds affecting approximately 4.5 per 1000 population, as reported by Ding et al., in 2022. However, there is a lack of studies on the epidemiology of wound infections in India, and a literature review reveals no recent data on their prevalence or the exact impact on quality of life in the Indian context (Sharma et al., 2024). Wound infections classified into acute and chronic wound infections. Acute wounds like cuts, burns, abrasions, and surgical wounds heal within 14 days, depending on size, type, wounded site, as well as the patient's age. In contrast, chronic wounds are more complicated than acute ones and take longer to heal. Chronic wounds are most often life threatening in elderly people, diabetic patients, obese and malnourished persons, and persons with vascular disease (Ding et al., 2022). In chronic wounds, several bacteria play significant roles in complicating wound healing, such as *Staphylococcus epidermis, Staphylococcus pseudintermedius, Staphylococcus aureus,* coagulase-negative *Staphylococcus aureus, Pseudomonas olevorans, Pseudomonas aeruginosa, Enterococcus faecalis, Klebsiella pneumonia, Streptococcus agalacteae, Streptococcus pyogenes, Escherichia coli, Morganella morganii, Providencia retgerii, Serratia rubidaea, Enterobacter aerogens* and *Enterobacter cloaceae* (Rajalakshmy et al., 2024).Compared to other pathogens, *S. aureus is* a versatile pathogen that causes a wide range of infections, including acute and chronic infections that can lead to life-threatening systemic diseases. The methicillin-resistant organism poses a global public health risk because of poor containment and treatment choices that result in higher global mortality rates. To combat these diseases, we need to develop an alternative to antibiotics (Almuhayawi et al., 2023).

Nanomedicine is one of the important applications of nanoparticles (10-100 nm in size) or their derivatives used for infection control, medical diagnosis, and drug delivery. Various nanoparticles were explored over the last two decades due to their wide applications to mitigate issues in human society by target specificity. Intense nanoparticle applications have significant breakthroughs and novel paradigms in the control of emerging pathogens. Hence the demand for nanoparticles is increasing in various fields, especially in biomedical applications. Iron oxide nanoparticles (IONP) were the first kind of metal nanoparticles authorized by the US Food and Drug Administration and the European Medicines Agency for clinical or preclinical studies. IONP

is used extensively in the biomedical disciplines for targeted drug delivery, cancer immunotherapy, and magnetic resonance imaging (MRI) because of their strong magnetism, lower toxicity, and good biocompatibility (Meng et al., 2024). Hence this study aimed to use IONP to treat drug-resistant pathogens.

Recently, molecular docking has gained more attention due to the computational capacity to forecast the binding energies and interactions between proteins and drugs. The mechanism of inhibition by iron oxide nanoparticles against MDR pathogens was evaluated by *in silico* docking analysis. Various studies published previously to determine the interaction of nanoparticles with respective proteins (El-Sayed et al., 2024) (Chibber & Ahmad, 2016). Various researchers reported that due to nanosized nanoparticles being able to penetrate into bacterial cells through cell walls, it leads to leakage of bacterial organelles to explore the interaction of IONP with bacterial surfaces or cell wall surface proteins selected. This study aims to develop IONP based nanomedicine to combat multidrug-resistant wound infections caused by *S. aureus*.

Materials and methods

Synthesize of IONP by co precipitation method

About 50 ml of 2M Ferrous sulfate (FeSO4.7H2O) and 1M Ferric chloride (FeCl3.6H2O) solutions were prepared and mixed with continuous stirring at 35˚C. After complete dissolution, 0.2M NaOH was added dropwise into the mixture at 45˚C with vigorous stirring until it reached alkaline pH. To identify the optimum pH for maximizing the IONP production, the pH of the solution was set to 8, 9, 10, and 11. Precipitated content was stirred for 2 hours at 60˚C and allowed to stand for 50 minutes and centrifugation at 1000 rpm for 10 minutes. Collected material washed repeatedly until it reaches neutral pH, air-dried, and stored in an air-tight container (Abbad et al., 2022).

Characterization of IONP

UV-Visible spectrophotometry

Nanoparticles dispersed in deionized water at a concentration of 1mg/ml. The UV-visible spectra of the sample were recorded at the 200-800nm range using a JASCO UV-Visible V-730 spectrophotometer (Andrade-Zavaleta et al., 2022).

Stability determination - Zeta potential analysis

Stability and surface charge of IONP determined by Zeta sizer version 6.32 (Malvern instruments). A clear disposable zeta cell electrode was introduced into the IONP sample at 1mg/ml concentration to create an electric field. The mean value of 24 consecutive zeta potential measurements runs at 25˚C expressed as the zeta potential of IONP (Singh et al., 2020).

Field Emission Scanning Electron Microscopy (FESEM)

The size and shape of IONP characterized using MIRA3 TESCAN. FESEM analysis was used with high-resolution imaging to provide detailed insights into the morphology of the IONP (Hui and Salimi, 2020).

Fourier transform infrared spectrophotometry

Functional groups and molecular bonds of synthesized IONP identified using JASCO FT/IR-4600. About 10µg of IONP placed on ATR plate, pressure clamp was adjusted to make contact with the sample and measured at a wavelength of 600-4000 cm-1 at a resolution of 4 cm- 1 (Karpagavinayagam and Vedhi, 2018).

Culture collection and preparation of inoculum

Wound infection-causing pathogens of S. aureus, E. faecalis, E. coli, K. pneumonia and P. aeruginosa procured from United Laboratories, Tirupur, India. Before antimicrobial activity determination, collected pathogens were subcultured in nutrient broth and incubated overnight at 37˚C (Abolarinwa et al., 2024).

Preparation of nanoparticles suspension

Suspension of IONP prepared by adding 1000µg of IONP/ml of dimethyl sulfoxide (DMSO) and sonicated for 30 minutes to achieve a homogenous solution (Abolarinwa et al., 2024).

Antibacterial activity of IONP against pyogenic pathogens

The antibacterial activity of IONP was determined against collected pathogens, including *S. aureus, P. aeruginosa, E. coli, K. pneumoniae*, and *E. faecalis* by well diffusion method. Overnight cultures of pathogens were swabbed on Mueller-Hinton agar plates using sterile cotton swabs. Plates were left for 10 minutes for culture absorption followed by 6 wells formed into which 10, 20, 30, 40, and 50µg/ml of IONP loaded with sterile micropipettes. Vancomycin 30mcg and Imipenem 10mcg served as positive controls, while DMSO used as negative control, inoculated plates incubated at 37°C for 24 hours. Following incubation, the zone of inhibition was measured in millimeters. Antibacterial activity of IONP by well diffusion method was performed thrice to ensure accuracy (Klink et al., 2022).

Minimum inhibitory Concentration (MIC)

MIC of IONP determined by broth dilution assay against pyogenic pathogens. About 1ml of sterile nutrient broth was taken in sterile test tubes and 1ml of IONP at 1mg/ml added into the tubes and serial dilution was carried out to prepare 500, 250, 125, 62.5, 31.25, 15.62, 7.81 and 3.75µg concentrations. Tubes inoculated with 10µl of culture inoculum, and nutrient broth along with 10µl of test cultures were used as positive control whereas; nutrient broth itself was used as negative control. Tubes were incubated at 37˚C for 24 hours and observed for turbidity after incubation (Mubaraki et al., 2024).

Minimum bactericidal concentration (MBC)

MBC was performed to determine the minimum concentration of IONP required to kill the pathogens. MBC was determined followed by MIC experiment, 10µl of broth was taken from each MIC tube and streaked on nutrient agar plates. Plates incubated at 37˚C for 24 hours and observed. Minimum concentration of IONP with the absence of bacterial growth is considered as MBC (Mubaraki et al., 2024).

Antioxidant Assay (2, 2-Diphenyl-1-Picrylhydrazyl (DPPH))

Antioxidant activity of IONP evaluated by slightly modified method of Kunjan et al., proposed technique in 2024. About 0.1mM DPPH solution prepared using methanol and 100µl of IONP solution prepared using distilled water. About 3ml of DPPH and nanoparticles solution mixed and incubated at dark for 30 minutes. Color change from purple to yellow recorded after 30 minutes. Absorbance recorded at 517nm using UV Visible spectrophotometry. Concentrations

ranging 10-100µg of ascorbic acid used as positive control and standard curve drawn accordingly (Tabassum et al., 2023).

ADMET properties determination

Swiss ADME and ADMET SAR online tools used to forecast the pharmaceutical and toxicological features, such as adsorption, distribution, metabolism, excretion, and toxicity. The pharmaceutical properties, such as the molecular formula, molecular weight, number of heavy atoms, number of aromatic heavy atoms, number of rotatable bonds, number of H-bond acceptors, number of H-bond donors, MR, TPSA, Consensus log P, and Ali class, determined using Swiss ADME in conjunction with Lipinski's rule of five. The blood-brain barrier, human intestinal adsorption, CaCO2 permeability, carcinogenicity, and acute oral, fish, honey bee, and rat toxicity were evaluated using the ADMETSAR online tool. The characteristics of ADMET predicted by the SMILES of ligands obtained from Pubchem database (Mohammed et al., 2023).

Preparation of protein and ligand

Interaction of IONP with surface protein G of S. aureus determined by molecular docking. The 3D structure of the S. aureus surface protein G (target protein) 3TIP and 3TIQ obtained in PDB format from the RCSB PDB database and subsequently prepared using Discovery Studio v24.1.0.23298. During protein preparation, water molecules and hetero atoms were removed, and polar hydrogens merged. Ligand (Fe3O4) structure drawn by Chemsketch (Freeware) 2023.2.4 converted into 3D and its energy minimized using Open Babel (available within PyRx) and then converted to PDBQT format (Umar et al., 2021).

Molecular docking

Molecular docking a computational technique used for various purposes, including drug design and discovery, the identification of biomolecule interactions etc. Molecular interaction between IONP and S. aureus surface protein G 3TIP and 3 TIQ analyzed using PyRx 0.8 software. Once the protein and ligand prepared, loaded into PyRx for docking analysis. Grid box configured to cover the entire protein before proceeding with the docking. Followed by docking, results recorded in a CSV format using Microsoft Excel, and the interactions between the target protein and ligand visualized in Discovery Studio (Mohammadjani et al., 2023)

RESULT AND DISCUSSION

Synthesis of iron nanoparticles

Compared to other methods of nanoparticle synthesis, the co-precipitation method was easy and efficient, and the size and form of the nanoparticles were regulated by pH, salt type, and ionic strength (A et al., 2016).). From 10.7g of ferrous sulfate and ferric chloride about 7.5g IONP obtained which accounts for 70% yield. IONP synthesized under pH 10 resulted in small, black-colored, fine particles whereas; other pH resulted in comparatively large, coarse and aggregated particles (Fig. 1.). In comparison with physical and green synthesis methods, the co-precipitation method resulted in a higher yield of nanoparticles (Besenhard et al., 2020). Following the sequential chemical reaction summarized by Ba-Abbad et al., 2022,$Fe^{2+} + 2OH^- \rightarrow Fe(OH)_2$

$$4\ Fe(OH)_2 + O_2 \rightarrow 4\ FeOOH + 2H_2O$$

$$Fe(OH)_2 + 2FeOOH \rightarrow Fe_3O_4 + 2H_2O$$

$$Fe^{3+} + 3OH^- \rightarrow Fe(OH)_3$$

$$Fe(OH)_2 + 2Fe(OH)_3 \rightarrow Fe_3O_4 + 4H_2O$$

Fe_3O_4 might further oxidize into 3Fe (OH) 3+ hence, IONP usually coated with polymers or by any organic/inorganic molecules.

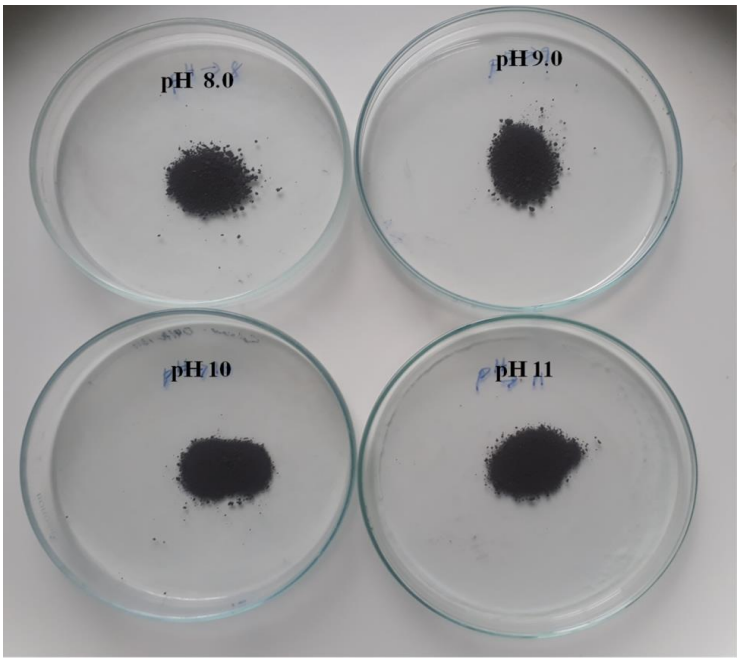

Fig. 1 Synthesized IONP

Characterization of nanoparticles

UV-Visible spectroscopy

Formation of IONP primarily confirmed by UV-visible spectroscopic analysis. IONP synthesized under different pH showed a prominent peak at 370 nm (Graph. 1.). Highest absorbance of 0.309 was recorded for IONP synthesized at pH 10. Hence, the nanoparticles synthesized under pH 10 taken for further analysis. Mubaraki et al in 2024 reported IONP showed an intense peak at 320nm due to surface plasmon excitation. Similar to our results recorded by Faisal et al., 2023.

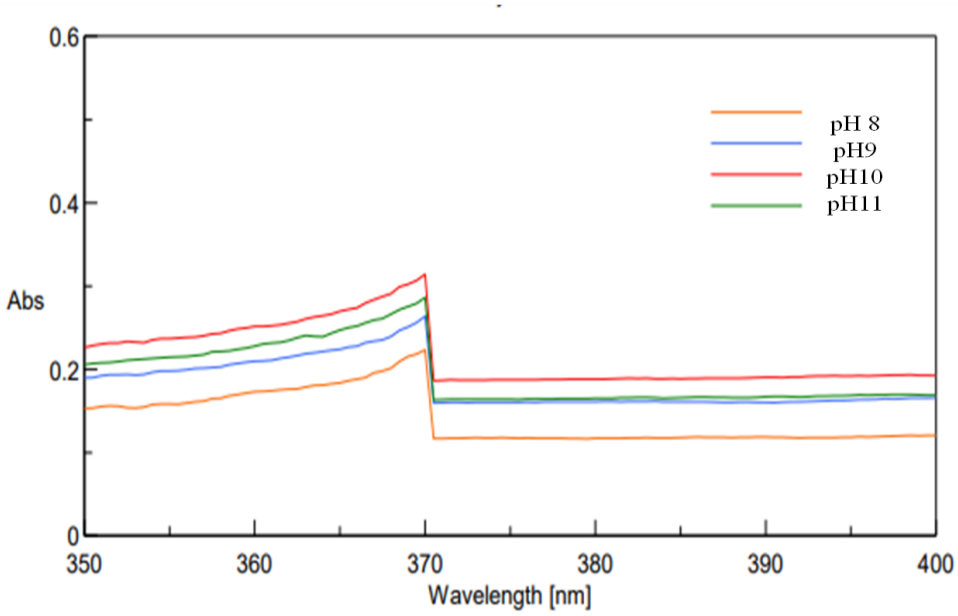

Graph. 1 UV-Vis Spectra of IONP

Zeta potential analysis

Electric charge on the surface of nanoparticles determined by the Zeta potential, which directly correlated with the stability of the nanoparticles. Substances with a zeta potential of more than 30mV considered to be highly stable, while those with a potential of less than 30mV tend to clump together or flocculate because of the attraction by Van der Waals interactions between particles (Demirezen et al., 2022). Zeta potential of the synthesized IONP calculated as -5.758mV (Graph. 2) revealed the lower stability of synthesized IONP in aqueous medium. High oxidation

tendency of IONP might be the factor for unstable nature. Singh et al in 2020 also reported IONP with low stability with -19.5mV zeta potential.

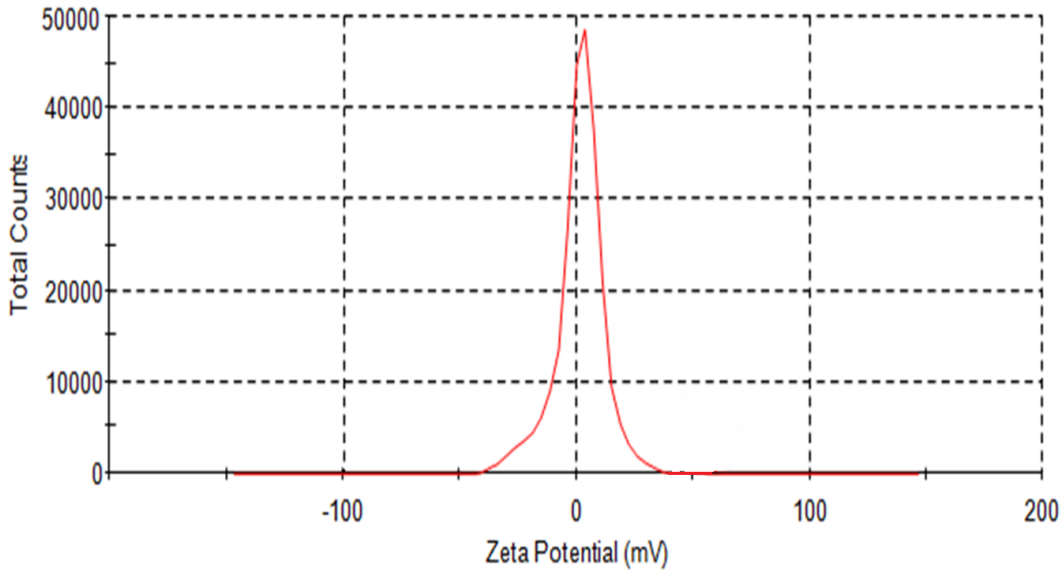

Graph. 2 Zeta potential spectra of IONP

FESEM ANALYSIS

FESEM analysis was further performed to determine the size and morphology of synthesized nanoparticles shown in Fig. 2. Under FESEM, co-precipitated nanoparticles observed as thin flakes-like structures 20.41 - 36.86nm in length and breadth. Similar structural spectrum of IONP interpreted by Faisal and co-workers in 2023. Similarly, the Spherical structure of IONP previously reported by Abolarinwa et al. 2024 discussed its oxidative nature under aerobic conditions.

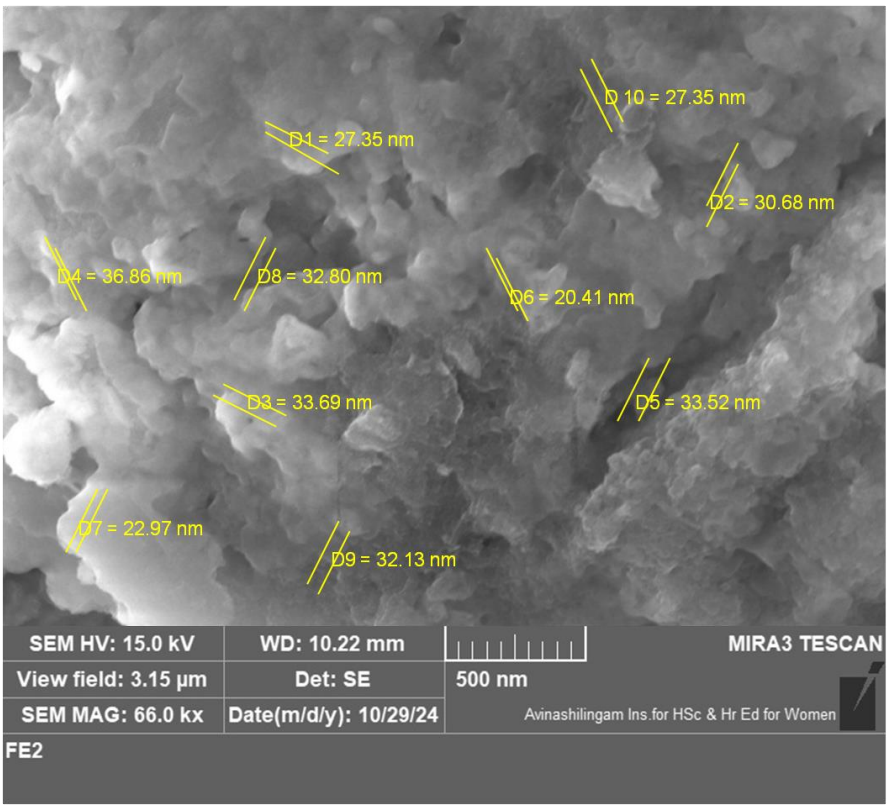

Fig. 2 FESEM observation of IONP

FTIR ANALYSIS

Obtained FTIR spectrum and its corresponding groups for IONP represented in Graph. 3. and table. 1. A weak peak at 3749.9 cm^{-1} indicated the presence of -OH groups. Broad peak at 3279.36 cm^{-1} represented the presence of Fe-O stretch which formerly reported by Jaha et al., 2024. Stretches at 1626.66 and 1541.81 cm^{-1} indicated the incidence of water molecules absorbed during synthesis. A weak peak at 1466.82 cm^{-1} represented O-H bend due to hydroxyl group (Ali et al. 2016). A Stretches of O-H and H-O-H suitable to hydroxyl groups at the surface of nanoparticles absorbed during the synthesis at aqueous environment which commonly found in IONP (Demirezen et al., 2022).

Table 1 Functional groups of IONP

Peaks in cm^{-1}	Functional groups
3749.9	-OH stretch
3279.36	Fe-O Stretch
1626.66	H-O-H bend
1541.81	O-H stretch
1466.82	O-H bend

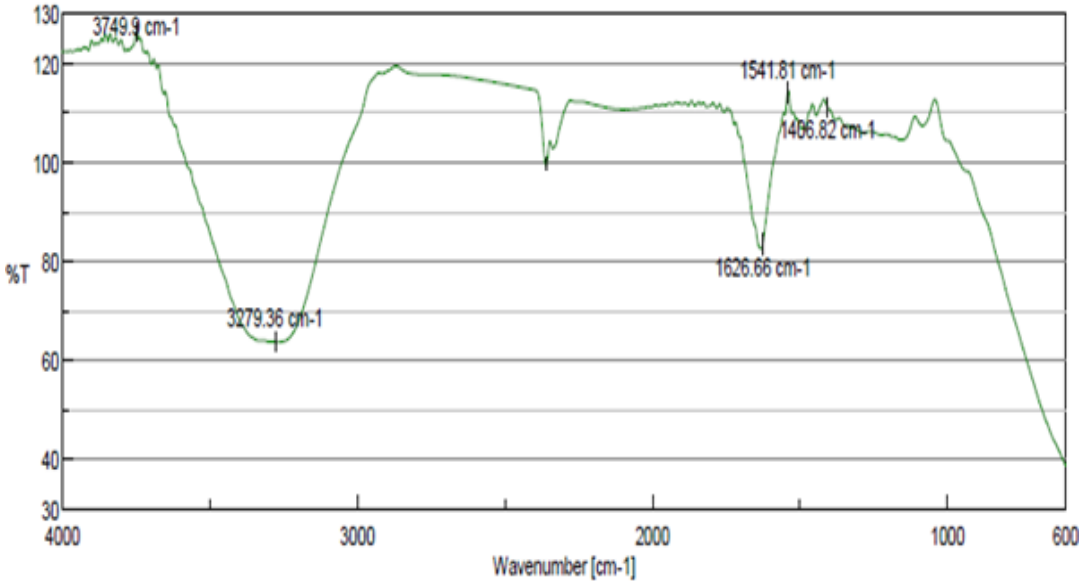

Graph. 3 FTIR spectrum of IONP

Antimicrobial activity of IONP.

Antimicrobial efficiency of IONP detected by well diffusion assay. About 50µg/ml IONP showed higher inhibition activities towards *S. aureus* with 20 ± 2 mm of zone of inhibition and lowest activity observed against *E. faecalis* with 12 ± 2 mm zone of inhibition (Fig. 3). IONP at 50 µg/mL showed more or less similar antibacterial activity against *E. coli*, *K pneumonia* and *P. aeruginosa* with 12 ± 2.08, 13 ± 2, and 13.33 ± 2.08 mm respectively (Table 2). The IONP exhibited concentration dependent result, with increasing concentrations leads to larger zones of inhibition (Graph. 4). IONP showed higher inhibitory towards *S. aureus* than other organisms

though it slightly lower than the inhibitory effect of standard antibiotic vancomycin 21 ± 2. Inhibitory activity of DMSO was negative. Results of this study revealed the potential of IONP as antimicrobial agents, as alternate to antibiotics particularly against Gram-positive pathogen as similar to the results obtained by Jaha et al., in 2024. However, to control MDR pathogens of Gram-negative bacteria the need further research to optimize IONP formulations and explore combination therapies to enhance their effectiveness against the resistant strains (Faisal et al., 2023). Due to nanoscale size of the particles, permeability of IONP into the bacterial cells are very high, which leads to structural damage of bacteria, by intracellular leakage, DNA damage or protein damage (Kunjan et al., 2024). Therefore antimicrobial effect of IONP could be integrated to membrane disruption or protein damage but, still research going on to elucidate the mode of action of IONP (Ezealigo et al., 2021).

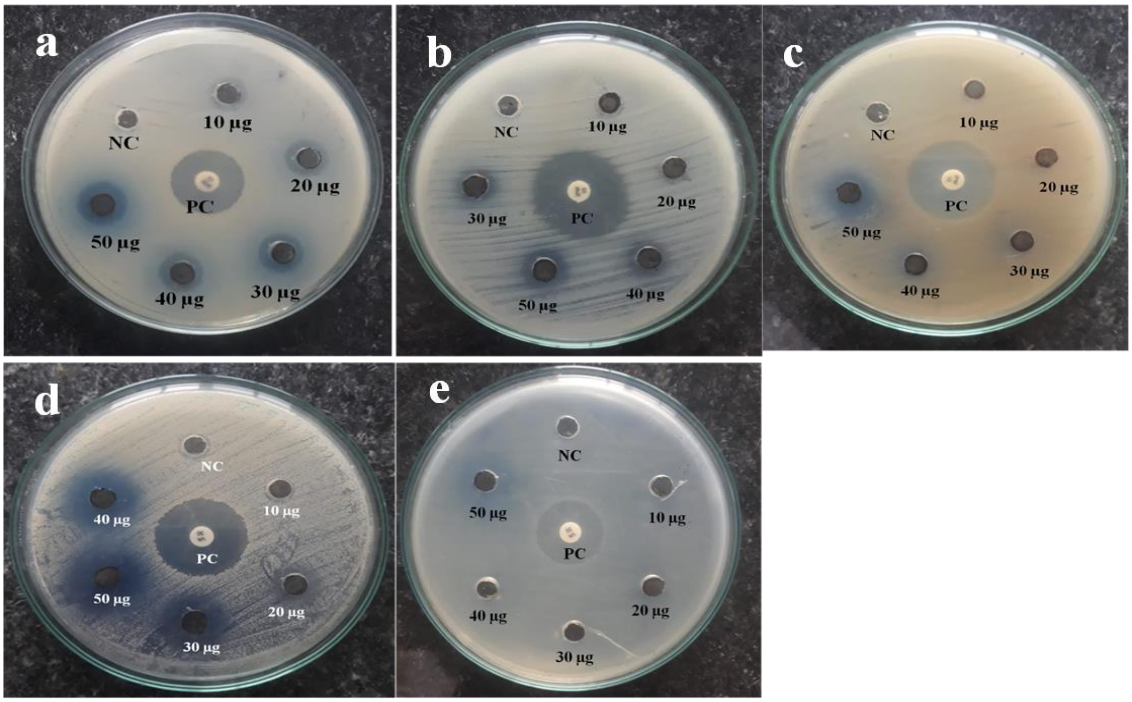

Fig. 3 Antimicrobial activity of IONP by well diffusion assay a) *E. coli* b) *K. pneumoniae* c*) P. aeruginosa* d) *S. aureus* e) *E. faecalis*

Table 2 Antimicrobial activity of IONP against pyogenic pathogens expressed as zone of inhibition ± SD

Concentration of nanoparticles in µg/ml	**Zone of inhibition (mm in diameter)**				
	E.coli	***K. pneumoniae***	***P. aeruginosa***	***S. aureus***	***E. faecalis***
10	5 ± 0.57	0 ± 0	0 ± 0	6.33 ± 2	0 ± 0
20	6.3 ± 2.08	6.3 ± 1.5	5.66 ± 1.15	11 ± 1.5	0 ± 0
30	8 ± 1	8.33 ± 2.08	6 ± 1	15 ± 2.08	0 ± 0
40	10 ± 1	10.33 ± 1.52	8 ± 1.52	18 ± 2	8 ± 1.52
50	12 ± 2.08	13 ± 2	13.33 ± 2.08	20 ± 2	12 ± 2
Positive control (Vancomycin/ Imipenem)	17 ± 1.15	21 ±1	23 ± 2	21 ± 2	19 ± 0.5

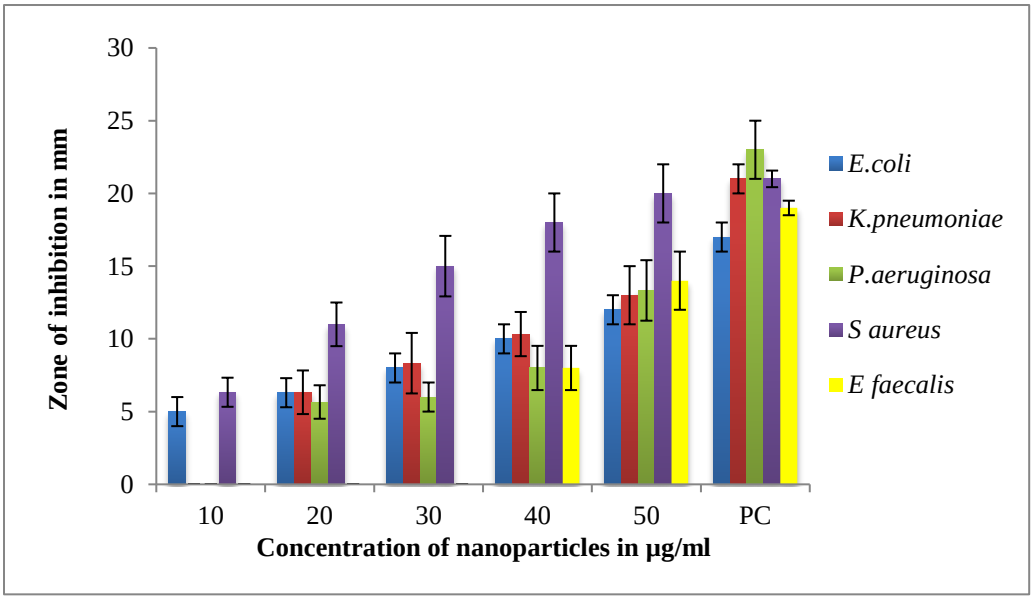

Graph. 4 Antimicrobial activity of IONP

MIC and MBC

Observed minimum concentration of IONP against pathogens shown in table 3. IONP showed inhibitory action at the minimum concentration of 31.25 µg/ml for *S. aureus* and *E. coli*, 62.5 µg/ml for *K. pneumonia* and *P. aeruginosa*, and 125 µg/ml for *E. faecalis*. Compared to Gram negative pathogens, Gram positive pathogens more susceptible at least (31.25 µg/ml) concentration of IONP and similar result obtained by Abolarinwa et al., in 2024 and Khatami et al., 2017. Bactericidal activity of IONP showed in table 3. At 62.5 µg/ml concentration, *E. coli* has shown no viable cells after 24 hours of incubation whereas 125 µg/ml for *K. pneumoniae,* 250 µg/ml for *P. aeruginosa* and *E. faecalis*, and 62.5 µg/ml for *S. aureus*. The outcomes were associated with studies of Jaha et al in 2024 reported double the concentration of MIC able to kill the pathogens effectively and MBC higher than MIC. Graphical representation OF MIC and MBC given in graph. 5.

Table 3 MIC and MBC results of IONP against bacterial pathogens

Organisms	**MIC (µg/ml)**	**MBC (µg/ml)**
E. coli	31.25	62.5
K. pneumoniae	62.5	125
P. aeruginosa	62.5	250
S. aureus	31.25	62.5
E. faecalis	125	250

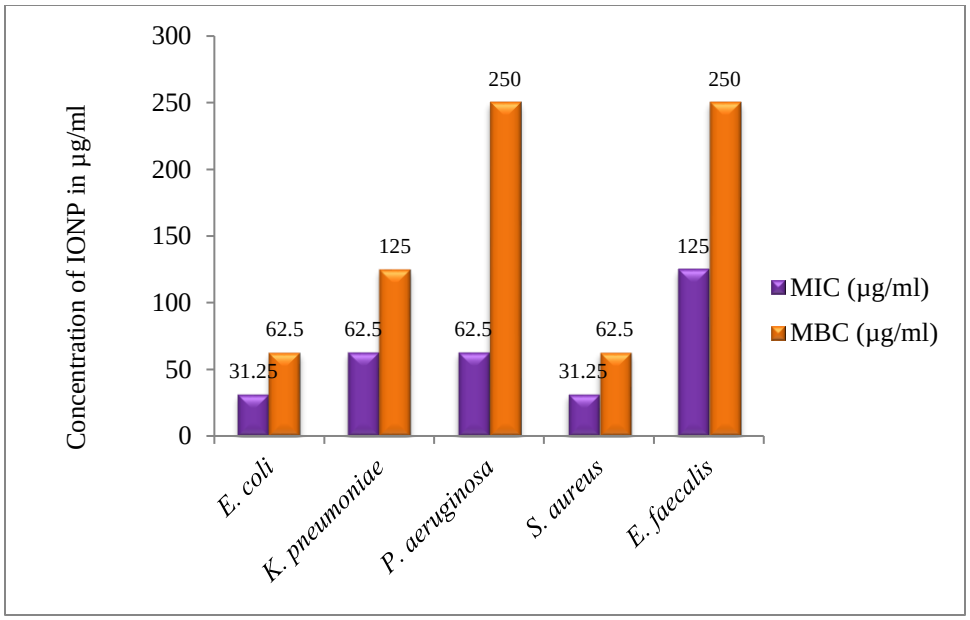

Graph. 5 MIC and MBC of IONP

Antioxidant activity (2, 2 -Diphenyl-1-Picrylhydrazyl (DPPH) Assay)

The DPPH (1,1-diphenyl-2-picrylhydrazyl) assay widely used method for evaluating the antioxidant activity. About 200 µl of IONP showed 61.4 µg of antioxidants. IONP showed significant color change from purple to yellow which indicated the presence of considerable antioxidants (Tabassum et al., 2023). When antioxidants in IONP, donates an electron or hydrogen atom to the DPPH radical, which results in color change from purple to yellow. The extent of this change was directly proportional to the antioxidant capacity of the IONP (Kunjan et al., 2024).

ADMET properties

Various pharmaceutical properties of IONP presented in Table. 4. From these properties, concluded that IONP adhere to Lipinski's Rule of Five, indicated favorable pharmacological characteristics as drug candidate. Fe_3O_4 molecular weight 231.53 g/mol, with 7 heavy atoms, has no hydrogen bond acceptors or donors and insoluble in water (A et al., 2016). Toxicological activity of Fe_3O_4 by ADMET SAR was shown in table. 5. Fe_3O_4 predicted to exhibit good blood-brain barrier (BBB) penetration, with a probability of 0.9354. It was also identified to have good absorption in the human intestine, with a probability of 0.7258. The $CaCO_2$ permeability results indicated moderate permeability, reflected in a probability of 0.5655. Furthermore, it has

probability of 0.5882 for low acute oral toxicity. Similar ADMET properties interpreted previously by Shah et al in 2022.

Table 4 ADMET characteristics of Iron oxide using SWISS ADME

Properties	Iron Oxide
Molecular formula	Fe_3O_4
Molecular weight	231.53 g/mol
Number of heavy atoms	7
Number of aromatic heavy atoms	0
Number of rotatable bonds	0
Number of H-bond acceptors	-
Number of H-bond donors	-
Molar refractivity	2.75
TPSA	0.00 $Å^2$
Consensus log P	-
Ali class	-

Table 5 Toxicological activity of Fe_3O_4 by ADMET SAR

Model	Result	Probability
Blood-Brain barrier	BBB+	0.9354
Human intestinal Absorption	HIA+	0.7258
$Caco_2$ Permeability	Caco2+	0.5655
AMES toxicity	Non AMES toxic	0.8735
Carcinogens	Carcinogens	0.5403
Fish toxicity	Low FHMT	0.8522
Honey bee toxicity	High HBT	0.7841
Acute oral toxicity	III	0.5882
Carcinogenicity	Non required	0.6246
Rat Acute toxicity	1.9047	LD50, mol/kg
Fish toxicity	1.2647	PLC50, mg/L

Molecular docking

Binding affinity between Fe_3O_4 and surface protein G 3TIP and 3TIQ (Fig. 3) calculated as -3.4 and -1.2 kcal/mol (Table 6.). This indicated higher affinity of IONP towards *S. aureus* surface protein G 3TIP. Iron oxide interacts with surface protein G 3 TIP through conventional H-bond with Glutamine A: 509, Arginine A: 507 and Valine A: 522, Carbon-Hydrogen bond with Histidine A: 506 and Aspartic acid A: 508, covalent bond with Lysine A: 546 (Fig. 4.). Iron oxide interacts with surface protein G 3 TIQ through threonine: 545 and Glutamine: 521 with Conventional H- Bond (Fig. 5). Among this two surface proteins, IONP showed high affinity towards *S. aureus* surface protein G 3TIP, confirmed by high binding affinity towards protein. Binding of IONP with surface protein and reducing its virulence by preventing adhesion to the host cell, preventing invasion in host, and evasion from host immune system could be the mode for its antimicrobial activity. From the predicted results it is possible to conclude that IONP as potential antimicrobial drug. Mohammed and co researchers in 2023 published binding affinity of -2.93 kcal/ mol has the potential to bind with the active site of the protein and inhibition. The current study revealed better binding affinity of -3.4 kcal/ mol, thus concluded its more antimicrobial efficacy.

Table 6 Results of molecular docking

Protein name	PDB ID	Bindig affinity kcal/mol	Interacting amino acid	Bond length
S. aureus surface protein G	3 TIP	-3.4	Glutamine A: 509	1.91
			Arginine A: 507	5.10
			Valine A: 522	1.93
			Histidine A: 506	3.09
			Aspartic acid A: 508	3.42
			Lysine A: 546	5.16
S. aureus surface protein G	3 TIQ	-1.2	Threonine 545	1.87
			Glutamine 521	2.39

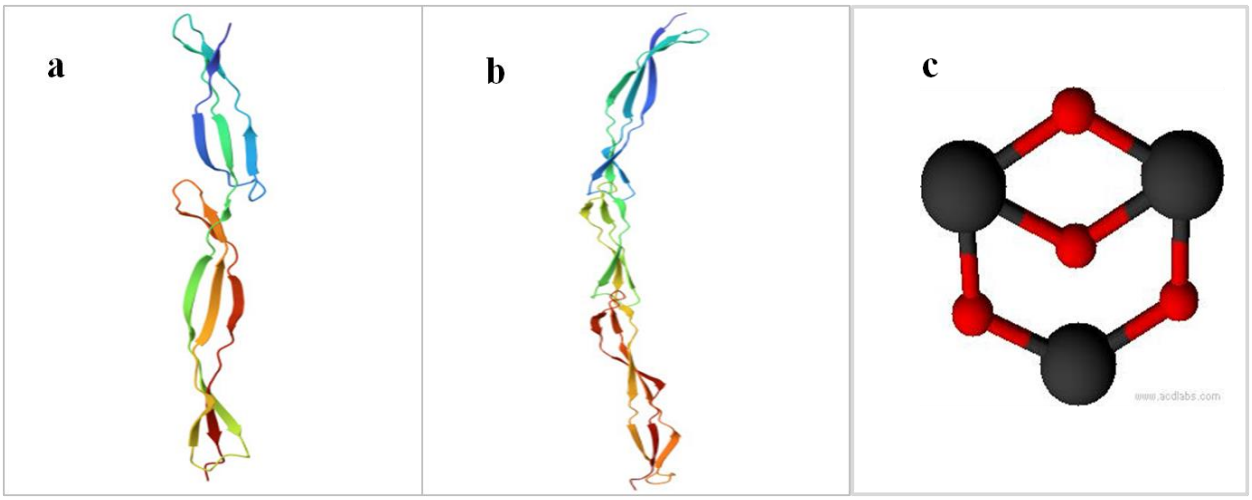

Fig. 4 Structure of target proteins and ligand a) *S. aureus* surface protein G 3TIP b) *S. aureus* surface protein G 3TIQ c) Chemical structure of Fe_3O_4 ligand

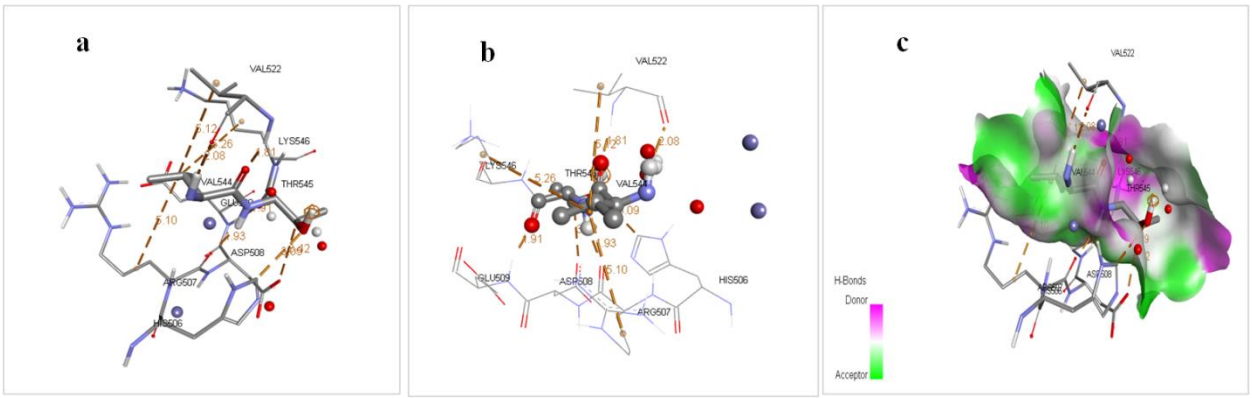

Fig. 5 Interaction of 3TIP with Fe_3O_4 ligand a) Protein ligand interaction in 3D b) Protein ligand interaction in ball and stick model c) Ligand protein interaction with H bond

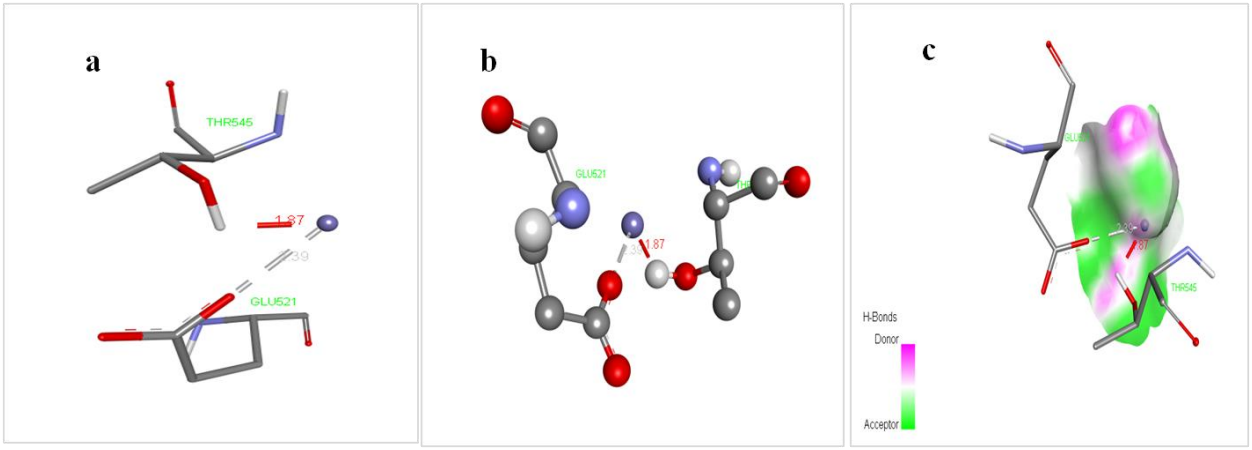

Fig. 6 Interaction of 3TIQ with Fe_3O_4 a) Protein ligand interaction in 3D b) Protein ligand interaction in ball and stick model c) ligand protein interaction with H bond

Conclusion

From the above-detailed research work, concluded that 70% IONP yield was achieved by the co-precipitation method at pH 10. IONP showed high absorbance at 370 nm. Zeta potential revealed, low stability due to the presence of negative charge in IONP. FESEM analysis exposed thin flakes-like structure of co-precipitated IONP and FTIR analysis indicated the presence of several functional groups with strong Fe-O stretch. In vitro, antimicrobial activity of IONP revealed high inhibition activity against methicillin-resistant S. aureus with 31.25 µg/ml MIC and 62.5 µg/ml MBC. A molecular docking study confirmed the high binding affinity of IONP with surface proteins of S. aureus, such as surface protein G3TIP. The study recommends the use of IONP at a lower concentration to target specific interactions and inhibit virulence of S. aureus as will be a good additive/substitute to commercially available antibiotics to overcome the infection caused by MRSA. By investigating the cytotoxic effect of synthesized IONP on S. aureus could suggest its promising role as nanomedicine against MDR pathogens.

Acknowledgement

The authors are grateful to RVS College of Arts and Sciences for providing laboratory facilities to conduct our research work. Special thanks to the DST-FIST for providing established instrumentation facility to complete the work at RVS College of Arts and Science, Coimbatore, India.

Funding

No funding was received for conducting this study.

Ethical approval

Not applicable.

Conflict of interest

The authors declare no conflict of interest.

Bibliography

Ali, A., Zafar, H., Zia, M., Haq, I. U., Phull, A. R., Ali, J. S., & Hussain, A. (2016). Synthesis, characterization, applications, and challenges of iron oxide nanoparticles. *Nanotechnology Science and Applications*, *Volume 9*, 49–67. https://doi.org/10.2147/nsa.s99986

Abolarinwa, T. O., Ajose, D. J., Oluwarinde, B. O., Montso, K. P., Fri, J., Fayemi, O. E., Aremu, A. O., & Ateba, C. N. (2024). Antimicrobial Properties and Cytotoxicity of Iron Oxide Nanoparticles Synthesized Using Melia azedarach Leaf Extract Against Diarrhoeal Pathogens. BioNanoScience, 0123456789. https://doi.org/10.1007/s12668-024-01393-1

Almuhayawi, M. S., Alruhaili, M. H., Gattan, H. S., Alharbi, M. T., Nagshabandi, M., Jaouni, S. A., Selim, S., Alanazi, A., Alruwaili, Y., Faried, O. A., & Elnosary, M. E. (2023). Staphylococcus aureus Induced Wound Infections Which Antimicrobial Resistance, Methicillin- and Vancomycin-Resistant: Assessment of Emergence and Cross Sectional Study. Infection and Drug Resistance, Volume 16, 5335–5346. https://doi.org/10.2147/idr.s418681

Andrade-Zavaleta, K., Chacon-Laiza, Y., Asmat-Campos, D., & Raquel-Checca, N. (2022). Green Synthesis of Superparamagnetic Iron Oxide Nanoparticles with Eucalyptus globulus Extract and Their Application in the Removal of Heavy Metals from Agricultural Soil. *Molecules*, *27*(4), 1367. https://doi.org/10.3390/molecules27041367

Ba-Abbad, M. M., Benamour, A., Ewis, D., Mohammad, A. W., & Mahmoudi, E. (2022). Synthesis of Fe3O4 Nanoparticles with Different Shapes Through a Co-Precipitation

Method and Their Application. Jom, 74(9), 3531–3539. https://doi.org/10.1007/s11837-022-05380-3

Besenhard, M. O., LaGrow, A. P., Hodzic, A., Kriechbaum, M., Panariello, L., Bais, G., Loizou, K., Damilos, S., Cruz, M. M., Thanh, N. T. K., & Gavriilidis, A. (2020). Co-precipitation synthesis of stable iron oxide nanoparticles with NaOH: New insights and continuous production via flow chemistry. Chemical Engineering Journal, 399, 125740. https://doi.org/10.1016/j.cej.2020.125740

Chibber, S., & Ahmad, I. (2016). Molecular docking, a tool to determine interaction of CuO and TiO 2 nanoparticles with human serum albumin. Biochemistry and Biophysics Reports, 6, 63–67. https://doi.org/10.1016/j.bbrep.2016.03.004

Demirezen, D. A., Yılmaz, Ş., Yılmaz, D. D., & Yıldız, Y. Ş. (2022). Green synthesis of iron oxide nanoparticles using Ceratonia siliqua L. aqueous extract: improvement of colloidal stability by optimizing synthesis parameters, and evaluation of antibacterial activity against Gram-positive and Gram-negative bacteria. International Journal of Materials Research, 113(10), 849–861. https://doi.org/10.1515/ijmr-2022-0037

Ding, X., Tang, Q., Xu, Z., Xu, Y., Zhang, H., Zheng, D., Wang, S., Tan, Q., Maitz, J., Maitz, P. K., Yin, S., Wang, Y., & Chen, J. (2022). Challenges and innovations in treating chronic and acute wound infections: from basic science to clinical practice. Burns & Trauma, 10. https://doi.org/10.1093/burnst/tkac014

El-Sayed, A. F., Aboulthana, W. M., Sherief, M. A., El-Bassyouni, G. T., & Mousa, S. M. (2024). Synthesis, structural, molecular docking, and in vitro biological activities of Cu-doped ZnO nanomaterials. Scientific Reports, 14(1). https://doi.org/10.1038/s41598-024-59088-2

Ezealigo, U. S., Ezealigo, B. N., Aisida, S. O., & Ezema, F. I. (2021). Iron oxide nanoparticles in biological systems: Antibacterial and toxicology perspective. JCIS Open, 4, 100027. https://doi.org/10.1016/j.jciso.2021.100027

Faisal, S., Sadiq, S., Mustafa, M., Khan, M. H., Sadiq, M., Iqbal, Z., & Khan, M. (2023). Tailoring the antibacterial and antioxidant activities of iron nanoparticles with amino benzoic acid. RSC Sustainability, 1(1), 139–146. https://doi.org/10.1039/d2su00044j

Hui, B. H., & Salimi, M. N. (2020). Production of Iron Oxide Nanoparticles by Co-Precipitation method with Optimization Studies of Processing Temperature, pH and Stirring Rate. IOP Conference Series: Materials Science and Engineering, 743(1). https://doi.org/10.1088/1757-899X/743/1/012036

Jaha, H. F., Anwar, Y., Al-Maaqar, S. M., Kamal, T., & Khan, S. B. (2024). Iron-Based Nanoparticles Synthesis, Characterization, and Antimicrobial Effectiveness. Advancements in Life Sciences, 11(2), 525–532. https://doi.org/10.62940/als.v11i2.3096

Karpagavinayagam, P., & Vedhi, C. (2018). Green synthesis of iron oxide nanoparticles using Avicennia marina flower extract. *Vacuum*, *160*, 286–292. https://doi.org/10.1016/j.vacuum.2018.11.043

Khatami, M., Aflatoonian, M. R., Azizi, H., Mosazade, F., Hooshmand, A., Lima Nobre, M. A., Minab Poodineh, F., Khatami, M., Khraazi, S., & Mirzaeei, H. (2017). Evaluation of Antibacterial Activity of Iron Oxide Nanoparticles Against Escherichia coli. International Journal of Basic Science in Medicine, 2(4), 166–169. https://doi.org/10.15171/ijbsm.2017.31

Klink, M. J., Laloo, N., Taka, A., Pakade, V., Monapathi, M., & Modise, J. (2022). Synthesis, Characterization and Antimicrobial Activity of Zinc Oxide Nanoparticles against Selected Waterborne Bacterial and Yeast Pathogens. Molecules, 27(11). https://doi.org/10.3390/molecules27113532

Kunjan, F., Shanmugam, R., & Govindharaj, S. (2024). Evaluation of Free Radical Scavenging and Antimicrobial Activity of Coleus amboinicus-Mediated Iron Oxide Nanoparticles. Cureus, 16(3), 1–10. https://doi.org/10.7759/cureus.55472

Meng, Y. Q., Shi, Y. N., Zhu, Y. P., Liu, Y. Q., Gu, L. W., Liu, D. D., Ma, A., Xia, F., Guo, Q. Y., Xu, C. C., Zhang, J. Z., Qiu, C., & Wang, J. G. (2024). Recent trends in preparation and biomedical applications of iron oxide nanoparticles. Journal of Nanobiotechnology, 22(1). https://doi.org/10.1186/s12951-023-02235-0

Mohammadjani, N., Karimi, S., Zorab, M. M., Ashengroph, M., & Alavi, M. (2023). Comparative molecular docking and toxicity between carbon-capped metal oxide nanoparticles and

standard drugs in cancer and bacterial infections. BioImpacts, 14(2), 27778. https://doi.org/10.34172/bi.2023.27778

Mohammed, Y. H. I., Alghamdi, S., Jabbar, B., Marghani, D., Beigh, S., Abouzied, A. S., Khalifa, N. E., Khojali, W. M. A., Huwaimel, B., Alkhalifah, D. H. M., & Hozzein, W. N. (2023). Green Synthesis of Zinc Oxide Nanoparticles Using Cymbopogon citratus Extract and Its Antibacterial Activity. ACS Omega, 8(35), 32027–32042. https://doi.org/10.1021/acsomega.3c03908

Mubaraki, M. A., Ali, J., Khattak, B., Fozia, F., Khan, T. A., Hussain, M., Aslam, M., Iftikhar, A., & Ahmad, I. (2024). Characterization and Antibacterial Potential of Iron Oxide Nanoparticles in Eradicating Uropathogenic E. coli. ACS Omega, 9(1), 166–177. https://doi.org/10.1021/acsomega.3c03078

Naghavi M, Stein Emil Vollset, Kevin S Ikuta, et al. GBD 2021 Antimicrobial resistance Collaborators. (2024). Global burden of bacterial antimicrobial resistance 1990-2021: a systematic analysis with forecasts to 2050. Lancet. 2024;404(10459):1199-226. doi:10.1016/S0140-6736(24)01867-1

Puca, V., Marulli, R. Z., Grande, R., Vitale, I., Niro, A., Molinaro, G., Prezioso, S., Muraro, R., & Di Giovanni, P. (2021). Microbial Species Isolated from Infected Wounds and Antimicrobial Resistance Analysis: Data Emerging from a Three-Years Retrospective Study. Antibiotics, 10(10), 1162. https://doi.org/10.3390/antibiotics10101162

Rajalakshmy, K., Kumari, S. P., & Ahmed, S. M. (2024). Prevalence and antibiogram of aerobic bacterial isolates from pus samples in a tertiary care hospital of north Kerala, India. Notulae Scientia Biologicae, 16(1), 11757. https://doi.org/10.55779/nsb16111757

Shabbir, M. A., Naveed, M., Rehman, S. U., Ain, N. U., Aziz, T., Alharbi, M., Alsahammari, A., & Alasmari, A. F. (2023). Synthesis of Iron Oxide Nanoparticles from Madhuca indica Plant Extract and Assessment of Their Cytotoxic, Antioxidant, Anti-Inflammatory, and Anti-Diabetic Properties via Different Nanoinformatics Approaches. *ACS Omega*, *8*(37), 33358–33366. https://doi.org/10.1021/acsomega.3c02744

Shah, S. T., Chowdhury, Z. Z., Johan, M. R. Bin, Badruddin, I. A., Khaleed, H. M. T., Kamangar, S., & Alrobei, H. (2022). Surface Functionalization of Magnetite Nanoparticles with Multipotent Antioxidant as Potential Magnetic Nanoantioxidants and Antimicrobial Agents. Molecules, 27(3). https://doi.org/10.3390/molecules27030789

Sharma, A., Srivastava, V., Shankar, R., Yadav, A. K., Ansari, M. A., & Gupta, S. K. (2024). Epidemiological profile of chronic wounds in an Indian population: a Community-Based Cross-Sectional Observational Study. Cureus. https://doi.org/10.7759/cureus.68684

Singh, K., Chopra, D. S., Singh, D., & Singh, N. (2020). Optimization and ecofriendly synthesis of iron oxide nanoparticles as potential antioxidant. Arabian Journal of Chemistry, 13(12), 9034–9046. https://doi.org/10.1016/j.arabjc.2020.10.025

Tabassum, N., Singh, V., Chaturvedi, V. K., Vamanu, E., & Singh, M. P. (2023). A Facile Synthesis of Flower-like Iron Oxide Nanoparticles and Its Efficacy Measurements for Antibacterial, Cytotoxicity and Antioxidant Activity. Pharmaceutics, 15(6). https://doi.org/10.3390/pharmaceutics15061726

Umar, H. I., Siraj, B., Ajayi, A., Jimoh, T. O., & Chukwuemeka, P. O. (2021). Molecular docking studies of some selected gallic acid derivatives against five non-structural proteins of novel coronavirus. Journal of Genetic Engineering and Biotechnology, 19(1). https://doi.org/10.1186/s43141-021-00120-7